

# Calculation of $\bar{B} \rightarrow D^* \ell \bar{\nu}$ form factor at zero recoil using the Oktay-Kronfeld action

Jon A. Bailey<sup>1</sup>, Tanmoy Bhattacharya<sup>2</sup>, Rajan Gupta<sup>2</sup>, Yong-Chull Jang<sup>2,3</sup>, Weonjong Lee<sup>1,\*</sup>, Jaehoon Leem<sup>1</sup>, Sungwoo Park<sup>1,\*\*</sup>, Boram Yoon<sup>4</sup>, and (LANL-SWME Collaboration)

<sup>1</sup>Lattice Gauge Theory Research Center, CTP, Department of Physics and Astronomy, Seoul National University, Seoul 08826, South Korea

<sup>2</sup>Los Alamos National Laboratory, Theoretical Division T-2, Los Alamos, New Mexico 87545, USA

<sup>3</sup>Brookhaven National Laboratory, Department of Physics, Upton, New York 11973, USA

<sup>4</sup>Los Alamos National Laboratory, Computer, Computational, Statistical Science Division CCS-7, Los Alamos, New Mexico 87545, USA

**Abstract.** We present the first preliminary results for the semileptonic form factor  $h_{A_1}(w=1)/\rho_{A_j}$  at zero recoil for the  $\bar{B} \rightarrow D^* \ell \bar{\nu}$  decay using lattice QCD with four flavors of sea quarks. We use the HISQ staggered action for the light valence and sea quarks (the MILC HISQ configurations), and the Oktay-Kronfeld (OK) action for the heavy valence quarks.

## 1 Introduction

The  $4.1\sigma$  tension between recently updated values of the exclusive and inclusive  $|V_{cb}|$  [1, 2], and the  $4.0\sigma$  tension between the standard model prediction of  $\varepsilon_K$  using the exclusive  $|V_{cb}|$  determined with lattice QCD inputs and the experimental value of  $\varepsilon_K$  [2] motivates higher precision lattice calculations of  $|V_{cb}|$ .

At present, the largest error in exclusive  $|V_{cb}|$  comes from the about 1% heavy quark discretization error in the Fermilab action used in current calculations [3]. To reduce this error, we are simulating the Oktay-Kronfeld action [4], which is an  $O(\lambda^3)$  improved version of the Fermilab action<sup>1</sup>. In this talk, we present the first results on the semileptonic form factor  $h_{A_1}(w=1)/\rho_{A_j}$  at zero recoil for the  $\bar{B} \rightarrow D^* \ell \bar{\nu}$  decay. The calculations were done on the  $a12m310$  2+1+1-flavor HISQ lattices generated by the MILC collaboration [5].

## 2 Nonperturbative determination of $K_{\text{crit}}$ , $K_c$ and $K_b$

The Oktay-Kronfeld (OK) action [4] is a highly improved version of the Fermilab action. It contains counter-terms up to  $\lambda^3$ , whereas the Fermilab action is improved only up to  $\lambda^1$  order. In both actions,

\*e-mail: wlee@snu.ac.kr

\*\*Speaker

<sup>1</sup>In the HQET power counting,  $\lambda \approx \Lambda/(2m_Q)$  where  $\Lambda \approx 300$  MeV and  $m_Q$  is the heavy quark mass. For the charm quark,  $\lambda \approx 1/8$  and for the bottom quark,  $\lambda \approx 1/30$ .

the bare quark mass is defined as

$$am_0 = \frac{1}{2u_0} \left( \frac{1}{\kappa} - \frac{1}{\kappa_{\text{crit}}} \right), \quad (1)$$

where  $u_0$  is the tadpole improvement factor determined from the  $1 \times 1$  Wilson loops. In case of the Fermilab action, the coefficients of the dimension 5 counter terms added for improvement are independent of  $m_0$ . It is therefore straight-forward to determine  $\kappa_{\text{crit}}$  by fitting the pion spectra with respect to  $am_0$ . In case of the OK action, some of the coefficients of the dimension 5 and dimension 6 counter terms, such as  $c_E$ ,  $c_1$ ,  $c_2 = c_3$ ,  $c_{EE}$  defined in [4], depend on  $m_0$  and  $\kappa_{\text{crit}}$ . Hence, for the OK action we determine  $\kappa_{\text{crit}}$  by iteration as described below.

1. First, we determine  $\kappa_{\text{crit}}^{\text{tree}}$  using the following formula:

$$\kappa_{\text{crit}}^{\text{tree}} = \frac{1}{2u_0 \cdot (1 + 3\zeta r_s + 18c_4)} = 0.053850 \dots \quad (2)$$

where we set  $\zeta = r_s = 1$  and  $c_4$  is given in Ref. [4]. For the HISQ ensemble with  $a \approx 0.12$  fm and  $M_\pi = 310$  MeV,  $a12m310$ , the quark masses are  $\{am_\ell, am_s, am_c\} = \{0.0102, 0.0509, 0.635\}$ .

2. Make an initial guess for  $\kappa_{\text{crit}}$ . We choose  $\kappa'_{\text{crit}} = 0.96\kappa_{\text{crit}}^{\text{tree}}$  based on Ref. [6], where it was shown that the nonperturbative  $\kappa_{\text{crit}}^{\text{NP}}$  is 4% smaller than  $\kappa_{\text{crit}}^{\text{tree}}$  for the Fermilab action.
3. Determine the OK action coefficients using  $\kappa'_{\text{crit}}$  and measure 2-point pion correlators with point sources and sinks. We use 3 different  $\kappa$  values such that pions have masses in the range of  $600 \leq m_\pi \leq 950$  MeV. Also, we investigate 9 different pion momenta  $\mathbf{p}$ .
4. We determine the pion kinetic mass,  $M_2$ , by fitting the ground state energy,  $E(\mathbf{p})$ , to the dispersion relation

$$E(\mathbf{p}) = M_1 + \frac{\mathbf{p}^2}{2M_2} - \frac{(\mathbf{p}^2)^2}{8M_4^3} - \frac{a^3 W_4}{6} \sum_{i=1}^3 p_i^4. \quad (3)$$

Here  $M_1$  is the rest mass,  $M_4$  is the quartic mass and  $W_4$  is the Lorentz symmetry breaking term.

5. Determine the new  $\kappa_{\text{crit}}$  by requiring  $A = 0$  in the quadratic fit to the following function:

$$M_2^2(\kappa, \kappa'_{\text{crit}}) = A + Bm_2(\kappa, \kappa_{\text{crit}}) + Cm_2^2(\kappa, \kappa_{\text{crit}}) \quad (4)$$

where the kinetic quark mass  $m_2$  is related to the  $m_0$  by the tree-level relation:

$$\frac{1}{am_2} = \frac{2\zeta^2}{am_0(2 + am_0)} + \frac{r_s \zeta}{1 + am_0}, \quad (5)$$

Since  $m_2(\kappa_{\text{crit}}, \kappa_{\text{crit}}) = 0$ ,  $M_2(\kappa, \kappa'_{\text{crit}})$  vanishes at  $\kappa = \kappa_{\text{crit}}$ .

6. Update  $\kappa'_{\text{crit}} = \kappa_{\text{crit}}$  and go back to step 3.

Fig. 1 shows the convergence of  $\kappa_{\text{crit}}$  as a function of the iteration number. After the two iterations, we declare convergence to  $\kappa_{\text{crit}}^{\text{NP}} = 0.051211(33)$  within statistical uncertainty. Further details will be reported in Ref. [7].

We measure the two point correlation functions for the  $B_s$  and  $D_s$  mesons (pseudo-scalar channel) using the OK action with the above nonperturbatively determined  $\kappa_{\text{crit}} = \kappa_{\text{crit}}^{\text{NP}}$ . To determine  $\kappa_c$  and  $\kappa_b$ ,

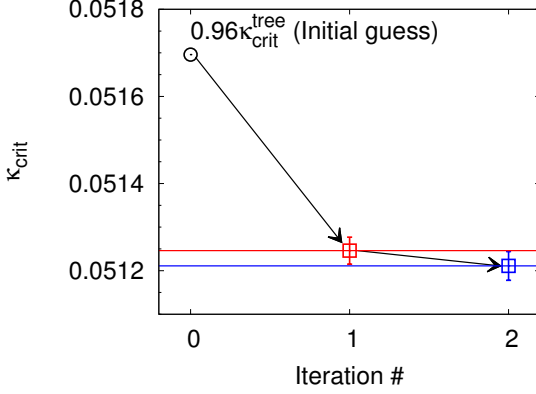


**Figure 1.**  $\kappa_{\text{crit}}$  as a function of the iteration number. The black circle is the initial guess, the red square is  $\kappa_{\text{crit}}$  after one iteration, and the blue square is the  $\kappa_{\text{crit}}$  after two iterations.

we simulate at four values of  $\kappa$  about estimates for the charm and the bottom quarks. For each  $\kappa$ , we obtain data for 11 momenta and determine the kinetic masses by fitting to the dispersion relation in Eq. (3). The final values of  $\kappa_c$  and  $\kappa_b$ , obtained by requiring the meson masses match the experimental  $B_s$  and  $D_s$  masses, are given in Table 1, for two determinations of the lattice spacing  $a$ ,  $a_{f_\pi^+}$  and  $a_{r_1}$ . Matching the pseudoscalar masses gives estimates with the smallest uncertainty.

**Table 1.** Results for  $\kappa_b$  and  $\kappa_c$ . The lattice spacing  $a$  is set in two ways: using  $a_{f_\pi^+} = 0.12520(22)$  fm from  $f_\pi^+$  in [8] and  $a_{r_1} = 0.1207(11)$  fm using  $r_1$  from [5]. The first error is statistical, the second is from the experimental error in  $M^X$ , and the third is a systematic error due to the fitting ambiguity.

(a) charm			(b) bottom		
X	$\kappa_c (a_{f_\pi^+})$	$\kappa_c (a_{r_1})$	X	$\kappa_b (a_{f_\pi^+})$	$\kappa_b (a_{r_1})$
pseudoscalar	0.048349(35)(9)(4)	0.048524(33)(43)(0)	pseudoscalar	0.04065(15)(2)(0)	0.04102(14)(9)(0)
vector	0.048338(62)(11)(0)	0.048533(59)(48)(1)	vector	0.04084(18)(2)(1)	0.04122(18)(10)(1)
spin-average	0.048341(51)(10)(1)	0.048531(48)(48)(1)	spin-average	0.04079(17)(2)(1)	0.04117(16)(10)(0)

### 3 Inconsistency

The inconsistency parameter  $I$  is defined as

$$I \equiv \frac{2\delta M_{\bar{Q}q} - (\delta M_{\bar{Q}Q} + \delta M_{\bar{q}q})}{2M_{2\bar{Q}q}} = \frac{2\delta B_{\bar{Q}q} - (\delta B_{\bar{Q}Q} + \delta B_{\bar{q}q})}{2M_{2\bar{Q}q}}, \quad (6)$$

where  $\delta M_X \equiv M_{2X} - M_{1X}$ , ( $X = \bar{Q}q, \bar{Q}Q$ ). In a relativistically invariant theory, the binding energy  $B_1$  is equal to  $B_2$ . The inconsistency  $I$  probes the binding energy difference  $\delta B = B_2 - B_1$ . This difference comes from the discretization errors in the  $O((ap)^4)$  terms of the action or in the  $O(v^4)$  in NRQCD power counting.  $I$  vanishes at tree level for the OK action, but not for the Fermilab action [6, 9].

In Fig. 2, we show  $I$  as a function of the pseudo-scalar heavy-light meson mass. Our previous results presented in Refs. [10–12] were obtained using the tree-level  $\kappa_{\text{crit}}^{\text{tree}}$  with asqtad strange quarks with point sources, while the results presented in Fig. 2 are obtained using the nonperturbatively determined  $\kappa_{\text{crit}}^{\text{NP}}$  with HISQ strange quarks with covariant Gaussian smearing applied to the heavy

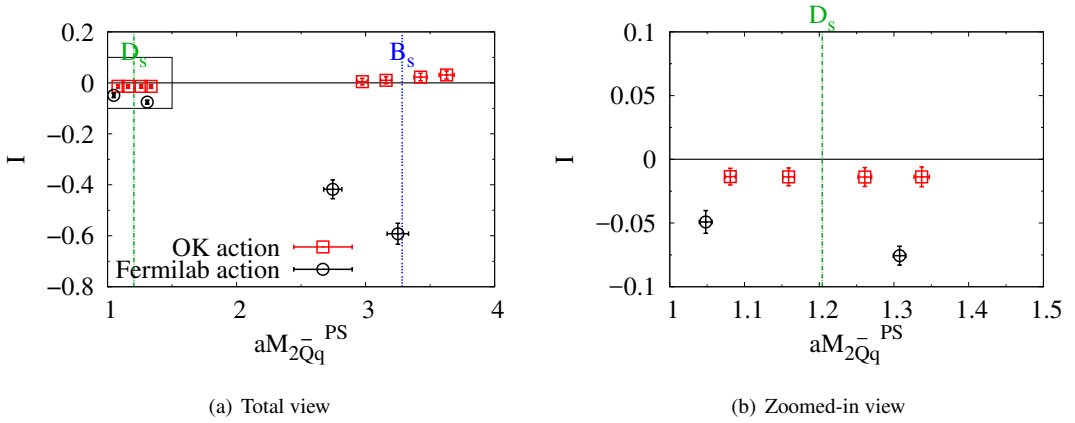


**Figure 2.** (a) Inconsistency parameter  $I$  as a function of pseudo-scalar heavy-light meson mass and (b) Zoomed-in view of the box near the  $D_s$  region. Here, we use  $\kappa_{\text{crit}}^{\text{NP}}$  to measure the 2-point meson correlation functions. The black circles represents results obtained using the Fermilab action with the asqtad strange quark. For more details, refer to Ref. [10]. The red squares represent results obtained using the OK action with the HISQ strange quark. Vertical dotted lines indicate the physical  $B_s$  and  $D_s$  pseudoscalar mesons.

quarks. We find that the inconsistency parameter vanishes within statistical uncertainty near the  $B_s$  region and it is smaller than that of Fermilab action by order of magnitude near the  $D_s$  region. This improvement is due to the combination of using the OK action on HISQ ensembles and smeared sources. It is observed for both  $\kappa_{\text{crit}}^{\text{tree}}$  and  $\kappa_{\text{crit}}^{\text{NP}}$ .

#### 4 Form factor $h_{A_1}(1)/\rho_{A_j}$ at zero recoil

To extract the form factor  $h_{A_1}(1)$  at zero recoil, we calculate the double ratio  $R$  on the lattice [13–15]:

$$R(t, t_f) \equiv \frac{C_{A_1}^{B \rightarrow D^*}(t, t_f) C_{A_1}^{D^* \rightarrow B}(t, t_f)}{C_{V_4}^{B \rightarrow B}(t, t_f) C_{V_4}^{D^* \rightarrow D^*}(t, t_f)} \xrightarrow[t \rightarrow \infty]{t_f \rightarrow \infty} \left| \frac{h_{A_1}(1)}{\rho_{A_j}} \right|^2 \xrightarrow[a \rightarrow 0]{V \rightarrow \infty} |h_{A_1}(1)|^2. \quad (7)$$

Here,  $\rho_{A_j}$  is the matching factor at  $a \neq 0$ .  $C_{J_\mu}^{X \rightarrow Y}(t, t_f)$  is a 3-point correlation function: for example, if  $X = B$ ,  $Y = D^*$  and  $J_\mu = A_j$ ,

$$C_{A_j}^{B \rightarrow D^*}(t, t_f) = \sum_{\mathbf{x}, \mathbf{y}} \langle O_j^{D^*}(0)^\dagger A_j^{cb}(\mathbf{y}, t) O^B(\mathbf{x}, t_f) \rangle \quad (8)$$

We define the axial and vector currents as follows:

$$\begin{aligned} A_j^{cb} &= \bar{\Psi}^c \gamma_j \gamma_5 \Psi^b, & V_4^{bb} &= \bar{\Psi}^b \gamma_4 \Psi^b \\ \Psi(x) &= \sum_{m=0} d_m \mathcal{R}_m \psi(x) \\ &= \left[ 1 + d_1 a \boldsymbol{\gamma} \cdot \mathbf{D} + d_2 a^2 \Delta^{(3)} + d_B a^2 i \boldsymbol{\Sigma} \cdot \mathbf{B} - d_E a^2 \boldsymbol{\alpha} \cdot \mathbf{E} + d_{rE} a^3 \{ \boldsymbol{\gamma} \cdot \mathbf{D}, \boldsymbol{\alpha} \cdot \mathbf{E} \} \right. \\ &\quad \left. - d_3 a^3 \sum_i \gamma_i D_i \Delta_i - d_4 a^3 \{ \boldsymbol{\gamma} \cdot \mathbf{D}, \Delta^{(3)} \} - d_5 a^3 \{ \boldsymbol{\gamma} \cdot \mathbf{D}, i \boldsymbol{\Sigma} \cdot \mathbf{B} \} \right] \end{aligned} \quad (9)$$

$$+ d_{EE} a^3 \{\gamma_4 D_4, \boldsymbol{\alpha} \cdot \mathbf{E}\} - d_6 a^3 [\gamma_4 D_4, \Delta^{(3)}] - d_7 a^3 [\gamma_4 D_4, i\boldsymbol{\Sigma} \cdot \mathbf{B}] \psi(x). \quad (10)$$

where  $d_0 = 1$ ,  $\mathcal{R}_0 = 1$ ,  $\mathcal{R}_1 = a\boldsymbol{\gamma} \cdot \mathbf{D}$ , and so on. Here,  $\Psi$  and  $\psi$  are improved and unimproved quark fields, respectively, and the coefficients  $d_m$  are real-valued analytic function of the bare mass  $am_0$  [16]. The currents are improved up to order  $\lambda^3$  at the tree level in the HQET power counting. We obtain the improved fields  $\Psi$  using the field rotation defined in Eq. (10). In short, using the field rotation is sufficient for the current improvement at the tree level [16–18].

We can rewrite the currents as follows,

$$A_j^{cb} = \bar{\Psi}^c \gamma_j \gamma_5 \Psi^b = \sum_{m,n=0} d_m(m_0^c) d_n(m_0^b) \bar{A}_{j,mn}^{cb} \quad (11)$$

$$\bar{A}_{j,mn}^{cb} \equiv \bar{\psi}^c \mathcal{R}_m^\dagger \gamma_j \gamma_5 \mathcal{R}_n \psi^b \quad (12)$$

and  $C_{A_j}^{B \rightarrow D^*}(t, t_f)$  as

$$C_{A_j}^{B \rightarrow D^*}(t, t_f) = \sum_{m,n=0} d_m(m_0^c) d_n(m_0^b) \bar{C}_{A_j;mn}^{B \rightarrow D^*}(t, t_f) \quad (13)$$

$$\bar{C}_{A_j;mn}^{B \rightarrow D^*}(t, t_f) \equiv \sum_{\mathbf{xy}} \langle O_j^{D^*}(0)^\dagger \bar{A}_{j,mn}^{cb}(\mathbf{y}, t) O^B(\mathbf{x}, t_f) \rangle. \quad (14)$$

There are 12 different rotation operators for  $\psi^b$  and  $\bar{\psi}^c$ . In total sum, we have  $144 = 12^2$  terms. However, some of them are  $O(\lambda^4)$ , which we exclude in this analysis. Hence, we end up with 30 terms up to  $O(\lambda^3)$ . Other 3-point functions occurring in Eq. (7) can be rewritten in a similar way.

In the measurements, we use point sources for the HISQ light quarks and choose their coordinates randomly. For the  $c$  and  $b$  quarks, we apply the covariant Gaussian smearing with  $(\sigma, N_{\text{GS}}) = (1.5, 5)$  at the source and sink points [19]. We also use the coherent source method [19] which gives a statistical gain by factor of 3 in the measurements. In the next subsections, we describe the extraction of  $R^{1/2} = h_{A_1}/\rho_{A_j}$  using two different analyses.

#### 4.1 Direct analysis on 3-point functions $C_{A_1}^{B \rightarrow D^*}$

The fitting function used for analyzing  $C_{A_1}^{B \rightarrow D^*}$  is

$$C_{A_1}^{B \rightarrow D^*}(t, t_f) = B^{B \rightarrow D^*} e^{-(M_B^* - M_B)t} e^{-M_B t_f} (1 + \hat{c}^{B \rightarrow D^*}(t, t_f)) \quad (15)$$

$$\bar{C}_{A_1;mn}^{B \rightarrow D^*}(t, t_f) = B_{mn}^{B \rightarrow D^*} e^{-(M_B^* - M_B)t} e^{-M_B t_f} (1 + \hat{c}_{mn}^{B \rightarrow D^*}(t, t_f)), \quad (16)$$

where  $B^{B \rightarrow D^*} = \langle D^* | A_1^{cb} | B \rangle$ ,  $B_{mn}^{B \rightarrow D^*} = \langle D^* | \bar{A}_{1,mn}^{cb} | B \rangle$ , and  $\hat{c}^{B \rightarrow D^*}$  and  $\hat{c}_{mn}^{B \rightarrow D^*}$  represent the contamination from the excited states of  $B$  and  $D^*$  mesons. Once we extract the  $B$  parameters from the data, we can obtain  $R$  using the following relation:

$$R = \frac{B^{B \rightarrow D^*} \cdot B^{D^* \rightarrow B}}{B^{B \rightarrow B} \cdot B^{D^* \rightarrow D^*}} = \left| \frac{h_{A_1}(1)}{\rho_{A_j}} \right|^2 \quad (17)$$

The amplitude  $B$  of 3-point correlation function with  $O(\lambda^p)$  improved current is

$$B = B_{00} + \sum_{(m,n) \neq (0,0)} d_m(m_0^c) d_n(m_0^b) B_{mn} = B_{00} \left[ 1 + \sum_{(m,n) \neq (0,0)} d_m(m_0^c) d_n(m_0^b) \frac{B_{mn}}{B_{00}} \right]. \quad (18)$$

The merit of Eq. (18) is that the ratio of  $B_{mn}/B_{00}$  can be obtained by a simple constant fit to the following ratio:

$$F_{mn}(t, t_f) \equiv \frac{\bar{C}_{A_j;mn}^{B \rightarrow D^*}(t, t_f)}{\bar{C}_{A_j;00}^{B \rightarrow D^*}(t, t_f)} = \frac{B_{mn}}{B_{00}} \left[ 1 + \hat{c}_{mn}^{B \rightarrow D^*}(t, t_f) - \hat{c}_{00}^{B \rightarrow D^*}(t, t_f) + \dots \right]. \quad (19)$$

We find that the corrections to the leading term, contamination from the excited states, are small and under control. In fact, we can further reduce the contamination using the following linear combination [14, 15]:

$$\bar{F}_{mn}(t, t_f) \equiv \frac{1}{2}F_{mn}(t, t_f) + \frac{1}{4}F_{mn}(t, t_f + 1) + \frac{1}{4}F_{mn}(t + 1, t_f + 1) \quad (20)$$

$$= \frac{B_{mn}}{B_{00}} (1 + \bar{c}_{mn}(t, t_f) - \bar{c}_{00}(t, t_f)) \quad (21)$$

The coefficients of contamination terms from the parity partners are suppressed by factor of  $1/2 \sim 1/12$  in  $\bar{c}_{mn}$  compared with  $\hat{c}_{mn}$ . Hence, once we determine  $B_{00}$  from the exponential fitting, the rest of analysis is just a simple fit of  $\bar{F}_{mn}$  to a constant. In Fig. 3 (a), we show results of fitting the  $\bar{F}_{11}^{B \rightarrow D^*}$

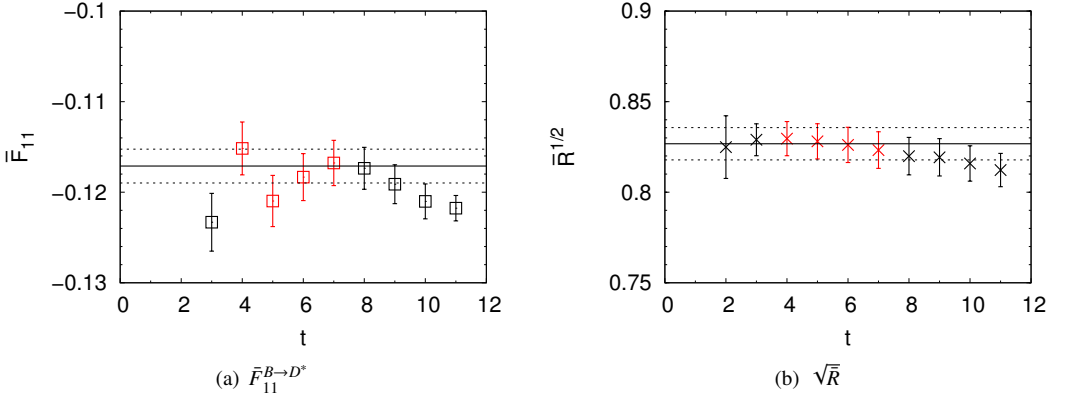


**Figure 3.** (a)  $\bar{F}_{11}^{B \rightarrow D^*}$  and (b)  $\sqrt{\bar{R}}$  as a function of time. Horizontal lines represent results of the constant fit. The red symbols represent those data points used for fitting. We use the  $O(\lambda^3)$  improved currents to obtain  $\bar{R}$ .

data to a constant as an example.

## 4.2 Analysis of $R$

By construction, the leading exponential dependence cancels out in the double ratio  $R$  defined in Eq. (7), so the correction due to the contamination from the excited states is further reduced. To further suppress this contamination, we take the same linear combination as for  $\bar{F}_{mn}$  in Eq. (20):

$$\bar{R}(t, t_f) \equiv \frac{1}{2}R(t, t_f) + \frac{1}{4}R(t, t_f + 1) + \frac{1}{4}R(t + 1, t_f + 1). \quad (22)$$

and fit the results to a constant. In Fig. 3 (b), we show results of fitting data for  $\sqrt{\bar{R}}$ , obtained using the currents improved up to  $O(\lambda^3)$ , to a constant.

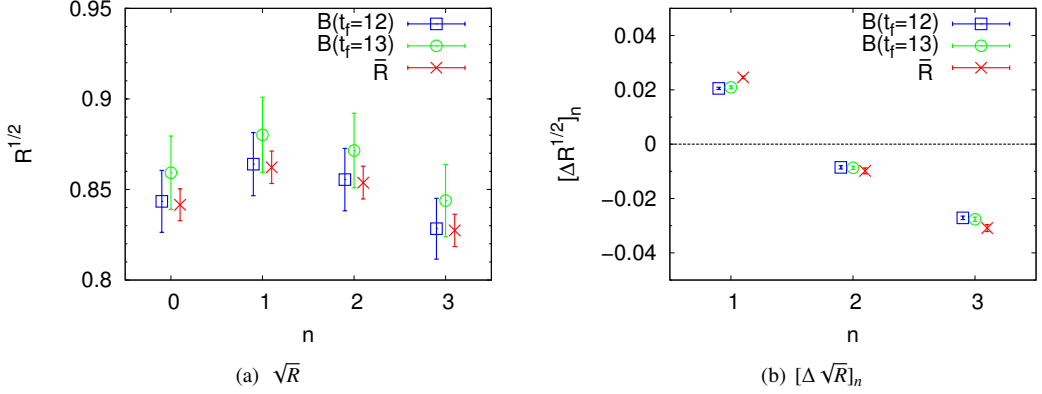


**Figure 4.** (a)  $\sqrt{R}$  as a function of  $n$ , and (b)  $[\Delta \sqrt{R}]_n$  as a function of  $n$ . Here,  $n$  represents the data points obtained using the currents improved up to  $O(\lambda^n)$ . Data for  $R$  at  $t_f = 12$  and  $t_f = 13$  is used to reconstruct  $\bar{R}$ .

In Fig. 4 (a), we present results for  $\sqrt{R}$  obtained in three different ways: (i) fit  $\sqrt{R}$  to a constant; (ii) obtain  $B_{00}$  by fitting the data at  $t_f = 12$  and combine it with results of  $\bar{F}_{mn}$ , and (iii) obtain  $B_{00}$  by fitting the data at  $t_f = 13$  and combining it with results of  $\bar{F}_{mn}$ . Results from the first method are given using red crosses, second method using blue squares, and the green circle for the third method. We find all three are consistent within statistical uncertainty.

To evaluate the corrections to  $\sqrt{R}$  from the improvement terms in the currents consider the quantity

$$[\Delta R^{1/2}]_n \equiv \frac{[R^{1/2}]_n - [R^{1/2}]_{n-1}}{[R^{1/2}]_{n-1}}. \quad (23)$$

where the subscript  $n$  in  $[R^{1/2}]_n$  represents results obtained using the currents improved up to  $O(\lambda^n)$ .

In Fig. 4 (b), we present results for  $[\Delta R^{1/2}]_n$  as a function of  $n$  with  $n = 1, 2, 3$  using the same convention for the symbols as in Fig. 4 (a). Due to a complicated structure of cancellation in the double ratio, we do not expect to see a simple scaling behavior in  $\lambda^n$  in  $[\Delta R^{1/2}]_n$ . However, we observe a kind of scaling behavior in  $[\Delta B]_n$  defined similarly as in Eq. (23). For a detailed analysis of these behaviors, we refer the reader to Ref. [7].

## Acknowledgment

We thank the MILC collaboration for sharing the 2+1+1-flavor HISQ ensembles generated by them. The research of W. Lee is supported by the Creative Research Initiatives Program (No. 2017013332) of the NRF grant funded by the Korean government (MEST). J.A.B is supported by the Basic Science Research Program of the National Research Foundation of Korea (NRF) funded by the Ministry of Education (No. 2015024974). W. Lee would like to acknowledge the support from the KISTI supercomputing center through the strategic support program for the supercomputing application research (No. KSC-2015-G2-002). The research of T. Bhattacharya, R. Gupta and Y-C. Jang is supported by the U.S. Department of Energy, Office of Science of High Energy Physics under contract number DE-KA-1401020, the LANL LDRD program and Institutional Computing. Computations were carried out in part on the DAVID clusters at Seoul National University.

## References

- [1] Y. Amhis et al. (2016), 1612.07233
- [2] Y.C. Jang, W. Lee, S. Lee, J. Leem, *Update on  $\varepsilon_K$  with lattice QCD inputs*, in *Proceedings, 35th International Symposium on Lattice Field Theory (Lattice2017): Granada, Spain*, to appear in EPJ Web Conf., 1710.06614
- [3] A.X. El-Khadra, A.S. Kronfeld, P.B. Mackenzie, Phys. Rev. **D55**, 3933 (1997), hep-lat/9604004
- [4] M.B. Oktay, A.S. Kronfeld, Phys. Rev. **D78**, 014504 (2008), 0803.0523
- [5] A. Bazavov et al. (MILC), Phys. Rev. **D87**, 054505 (2013), 1212.4768
- [6] C. Bernard et al. (Fermilab Lattice, MILC), Phys. Rev. **D83**, 034503 (2011), 1003.1937
- [7] J.A. Bailey, T. Bhattacharya, R. Gupta, Y.C. Jang, W. Lee, J. Leem, S. Park, B. Yoon et al. (LANL-SWME), *in preparation*
- [8] A. Bazavov et al. (Fermilab Lattice, MILC), Phys. Rev. **D90**, 074509 (2014), 1407.3772
- [9] A.S. Kronfeld, Nucl. Phys. Proc. Suppl. **53**, 401 (1997)
- [10] J.A. Bailey, Y.C. Jang, W. Lee, C. DeTar, A.S. Kronfeld, M.B. Oktay (2017), 1701.00345
- [11] J.A. Bailey, Y.C. Jang, W. Lee, C. DeTar, A.S. Kronfeld, M.B. Oktay, PoS **LATTICE2014**, 097 (2014), 1411.1823
- [12] J.A. Bailey, Y.C. Jang, W. Lee, C. DeTar, A.S. Kronfeld, M.B. Oktay, PoS **LATTICE2015**, 099 (2016), 1601.04759
- [13] S. Hashimoto, A.S. Kronfeld, P.B. Mackenzie, S.M. Ryan, J.N. Simone, Phys. Rev. **D66**, 014503 (2002), hep-ph/0110253
- [14] C. Bernard et al., Phys. Rev. **D79**, 014506 (2009), 0808.2519
- [15] J.A. Bailey et al. (Fermilab Lattice, MILC), Phys. Rev. **D89**, 114504 (2014), 1403.0635
- [16] J.A. Bailey, Y.C. Jang, W. Lee, J. Leem (LANL-SWME), *Improvement of heavy-heavy current for calculation of  $\bar{B} \rightarrow D^{(*)} \ell \bar{\nu}$  form factors using Oktay-Kronfeld heavy quarks*, in *Proceedings, 35th International Symposium on Lattice Field Theory (Lattice2017): Granada, Spain*, to appear in EPJ Web Conf., 1711.01777
- [17] J.A. Bailey, Y.C. Jang, W. Lee, J. Leem (SWME), PoS **LATTICE2014**, 389 (2014), 1411.4227
- [18] J.A. Bailey, J. Leem, W. Lee, Y.C. Jang, PoS **LATTICE2016**, 285 (2016), 1612.09081
- [19] B. Yoon et al., Phys. Rev. **D93**, 114506 (2016), 1602.07737